

# Stringent constraints on non-standard neutrino interactions using high-purity $\nu_\mu$ CC events in IceCube DeepCore

J Krishnamoorthi <sup>1,2</sup>, Anil Kumar <sup>1</sup> and Sanjib Kumar Agarwalla <sup>1,3</sup>

<sup>1</sup>*Institute of Physics, Sachivalaya Marg, Sainik School Post, Bhubaneswar 751005, India*

<sup>2</sup>*Department of Physics, Aligarh Muslim University, Aligarh 202002, India*

<sup>3</sup>*Homi Bhabha National Institute, Training School Complex, Anushakti Nagar, Mumbai 400094, India*  
krishnamoorthi.j@iopb.res.in, anil.k@iopb.res.in, sanjib@iopb.res.in

(Dated: December 30, 2025)

The neutral-current (NC) non-standard interactions (NSI) of neutrinos with fermions can modify the flavor oscillations of atmospheric neutrinos as they propagate through the Earth. We present constraints on the NC-NSI parameters  $\varepsilon_{\mu\tau}$  and  $\varepsilon_{\tau\tau} - \varepsilon_{\mu\mu}$  (one at a time) using a high-purity sample of  $\nu_\mu$  charged-current (CC) atmospheric neutrino events collected by IceCube DeepCore over 7.5 years of livetime. These two parameters significantly affect the  $\nu_\mu$  disappearance channel for which this golden event sample is optimized by the IceCube Collaboration. The best fit to this dataset is consistent with no NSI hypothesis, and we place the most stringent constraints to date:  $-0.0094 < \varepsilon_{\mu\tau} < 0.0079$  and  $-0.030 < \varepsilon_{\tau\tau} - \varepsilon_{\mu\mu} < 0.029$  at 90% confidence level.

**Introduction.**— The Nobel Prize in Physics (2015) was awarded for the discovery of neutrino oscillations [1–3], which provided direct evidence of non-zero neutrino mass, thereby requiring theories beyond the Standard Model (BSM) of particle physics. As we celebrate the tenth anniversary of this Nobel Prize, measurements of neutrino oscillation parameters have now entered into a precision era [4–6]. Over this decade, IceCube DeepCore [7] has emerged as a prominent atmospheric neutrino experiment, complementing the achievements of Super-Kamiokande [8]. With improved precision measurements of oscillation parameters, neutrinos provide a unique platform to search for new physics scenarios.

Considering the Standard Model (SM) of particle physics as an effective field theory [9] allows us to introduce the dimension-6 operator [10, 11] corresponding to new interactions of neutrinos beyond the SM. These non-standard interactions (NSI) of neutrinos were originally proposed by Wolfenstein [12] as a possible underlying mechanism behind neutrino flavor transitions. NSI could happen via charged current (CC) or neutral current (NC), which have been studied extensively in literature [13–51]. The CC-NSI affect the neutrino production and the detection, whereas the NC-NSI affect the neutrino propagation through matter. In this work, we utilize oscillations of atmospheric neutrinos passing through Earth to constrain the NC-NSI.

The effects of the NC-NSI can be incorporated in the neutrino oscillations by modifying the matter potential with the effective Hamiltonian in flavor basis given as

$$H_{\text{eff}} = \frac{1}{2E} U \begin{pmatrix} 0 & 0 & 0 \\ 0 & \Delta m_{21}^2 & 0 \\ 0 & 0 & \Delta m_{31}^2 \end{pmatrix} U^\dagger + V_{\text{CC}} \begin{pmatrix} 1 + \varepsilon_{ee} - \varepsilon_{\mu\mu} & \varepsilon_{e\mu} & \varepsilon_{e\tau} \\ \varepsilon_{e\mu}^* & 0 & \varepsilon_{\mu\tau} \\ \varepsilon_{e\tau}^* & \varepsilon_{\mu\tau}^* & \varepsilon_{\tau\tau} - \varepsilon_{\mu\mu} \end{pmatrix}, \quad (1)$$

where  $U$  is the Pontecorvo-Maki-Nakagawa-Sakata (PMNS) matrix [52],  $\Delta m_{ij}^2 \equiv m_i^2 - m_j^2$  are the mass-

squared differences, and  $V_{\text{CC}} \equiv \sqrt{2}G_F N_e$  [53, 54] represents the standard interaction (SI) potential due to the charged-current coherent forward scattering of neutrinos with the ambient electrons with number density  $N_e$ . The parameters  $\varepsilon_{\alpha\beta}$  are the NSI coupling parameters defined as  $\varepsilon_{\alpha\beta} = \varepsilon_{\alpha\beta}^e + 3\varepsilon_{\alpha\beta}^u + 3\varepsilon_{\alpha\beta}^d$ , representing contributions from interactions with electrons, up quarks, and down quarks, respectively. The diagonal parameters are real valued, whereas the off-diagonal parameters can be complex *i.e.*,  $\varepsilon_{\alpha\beta} \equiv |\varepsilon_{\alpha\beta}|e^{i\phi_{\alpha\beta}}$ , with  $\varepsilon_{\alpha\beta}^*$  denoting their complex conjugates. For antineutrinos,  $U \rightarrow U^*$ ,  $V_{\text{CC}} \rightarrow -V_{\text{CC}}$ , and  $\varepsilon_{\alpha\beta} \rightarrow \varepsilon_{\alpha\beta}^*$ .

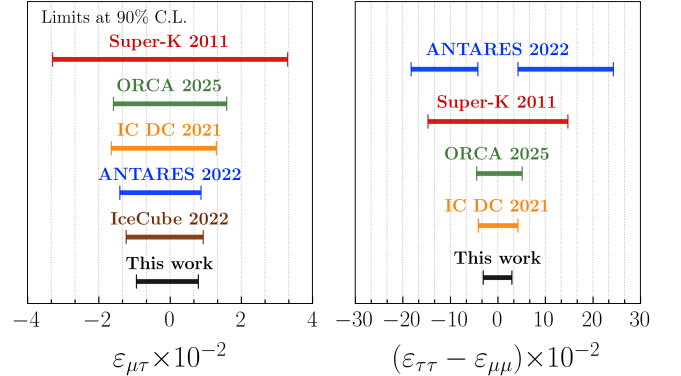


FIG. 1. Constraints on the NSI parameters  $\varepsilon_{\mu\tau}$  and  $\varepsilon_{\tau\tau} - \varepsilon_{\mu\mu}$  at 90% confidence level (C.L.) from this analysis using the 8-year golden event sample of IceCube DeepCore. Comparison with limits from other experiments, such as IceCube DeepCore (2021) [44], KM3NeT/ORCA (2025) [48], ANTARES (2022) [49], IceCube (2022) [50], and Super-Kamiokande (2011) [51] is shown. The limits for  $\varepsilon_{\mu\tau}$  are obtained by fixing the complex phase to 0 (*i.e.*, positive  $\varepsilon_{\mu\tau}$ ) and  $\pi$  (*i.e.*, negative  $\varepsilon_{\mu\tau}$ ). For consistency, bounds from Refs. [48–51] have been rescaled to the NSI convention used in our work.

In this work, we constrain the NC-NSI parameters  $\varepsilon_{\mu\tau}$  and  $\varepsilon_{\tau\tau} - \varepsilon_{\mu\mu}$  considering one at a time,

which significantly affect the  $\nu_\mu$  survival probability,  $P(\nu_\mu \rightarrow \nu_\mu)$ . To probe these parameters, we use a publicly available atmospheric neutrino dataset [55] from IceCube DeepCore with 7.5 years of livetime that is specifically optimized for  $\nu_\mu$  CC events. This high-purity  $\nu_\mu$  CC sample has an excellent sensitivity to the  $\nu_\mu$  disappearance ( $\nu_\mu \rightarrow \nu_\mu$ ) channel, which is expected to play an important role in probing the NSI parameters  $\varepsilon_{\mu\tau}$  and  $\varepsilon_{\tau\tau} - \varepsilon_{\mu\mu}$ . Throughout this work, we assume normal mass ordering. Figure 1 presents updated constraints on the NSI parameters  $\varepsilon_{\mu\tau}$  and  $\varepsilon_{\tau\tau} - \varepsilon_{\mu\mu}$  obtained using this 8-year golden event sample of IceCube DeepCore, and a comparison is done with the limits from the other neutrino oscillation experiments. Here, we treat  $\varepsilon_{\mu\tau}$  as a real parameter while deriving the corresponding limits. The constraints derived in this work represent the most stringent bounds to date. For comparison, we have included the results from several neutrino oscillation experiments like IceCube DeepCore [44], ORCA [48], ANTARES [49], IceCube [50], and Super-Kamiokande [51]. While the IceCube analysis utilized a TeV-energy atmospheric neutrino sample, the present study uses the lower-energy DeepCore data that are better suited for oscillation measurements. Our analysis procedure to obtain the above-mentioned constraints are described in detail in the later part of the letter. Let us first understand how the presence of NSI affects the neutrino oscillation patterns.

**Effects of NSI on neutrino oscillations.**— The presence of NSI modifies the effective matter potential experienced by neutrinos as they propagate through the Earth. This can lead to significant alterations in the oscillation probabilities, depending on the magnitude and sign of the NSI parameters. The following Eqn. 2 taken from the Ref. [43], shows the modified mixing angle  $\theta_{23}$  in matter due to the presence of NSI parameters  $\varepsilon_{\mu\tau}$  and  $\varepsilon_{\tau\tau} - \varepsilon_{\mu\mu}$ .

$$\tan 2\theta_{23}^m \simeq \frac{(c_{13}^2 - \alpha c_{12}^2) \sin 2\theta_{23} + 2\varepsilon_{\mu\tau}\hat{A}}{(c_{13}^2 - \alpha c_{12}^2) \cos 2\theta_{23} + (\varepsilon_{\tau\tau} - \varepsilon_{\mu\mu})\hat{A}}, \quad (2)$$

where  $\alpha = \Delta m_{21}^2/\Delta m_{31}^2$  and  $\hat{A} = V_{CC}/\Delta m_{31}^2$ . Considering one NSI parameter at a time, both  $\varepsilon_{\mu\tau}$  and  $\varepsilon_{\tau\tau} - \varepsilon_{\mu\mu}$  will be having an impact on the mixing angle  $\theta_{23}$  which could affect the probability amplitude. In addition, the NSI parameter  $\varepsilon_{\mu\tau}$  also modifies the parameter  $\Delta m_{31}^2$  [43], which results in a significant change in the location of the oscillation valley.

Figure 2 shows the effects of the NSI parameters  $\varepsilon_{\mu\tau}$  and  $\varepsilon_{\tau\tau} - \varepsilon_{\mu\mu}$  one at a time in the plane of neutrino energy and the cosine of zenith angle. The difference of probabilities  $P(\nu_\mu \rightarrow \nu_\mu)$  between SI + NSI and SI scenarios shows that the presence of  $\varepsilon_{\mu\tau} = \pm 0.05$  shifts the location of the oscillation valley, which results in the prominent alternative patches of blue and red. Additionally, the direction of shift in the oscillation valley depends on the sign of  $\varepsilon_{\mu\tau}$ . On the other hand,

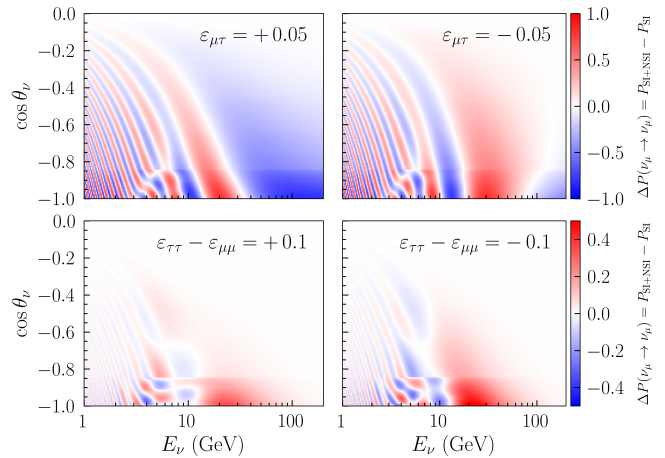


FIG. 2. Difference in the three-flavor neutrino oscillation probabilities  $P(\nu_\mu \rightarrow \nu_\mu)$  between SI + NSI and SI scenarios in the plane of neutrino energy and cosine of zenith angle. The top and bottom panels correspond to the NSI scenarios with  $\varepsilon_{\mu\tau} = \pm 0.05$  and  $\varepsilon_{\tau\tau} - \varepsilon_{\mu\mu} = \pm 0.1$ , respectively, considering one NSI parameter at a time. Here, we take  $\theta_{23} = 45.57^\circ$  and  $\Delta m_{31}^2 = 2.48 \times 10^{-3} \text{ eV}^2$ .

the presence of  $\varepsilon_{\tau\tau} - \varepsilon_{\mu\mu} = \pm 0.1$  mainly affects the mixing angle  $\theta_{23}$  and results in a modification in the depth of the oscillation valley. Note that the direction of this modification is independent of the sign of  $\varepsilon_{\tau\tau} - \varepsilon_{\mu\mu}$ . Comparing the effects of  $\varepsilon_{\mu\tau}$  and  $\varepsilon_{\tau\tau} - \varepsilon_{\mu\mu}$  on the oscillograms, the parameter  $\varepsilon_{\mu\tau}$  have impact up to high-energy regions, meanwhile the parameter  $\varepsilon_{\tau\tau} - \varepsilon_{\mu\mu}$  shows effect only below 100 GeV. To probe these two NSI parameters, we utilize a publicly available atmospheric neutrino data sample [55] collected during 2011-2019 by IceCube DeepCore.

**Neutrino events at IceCube DeepCore.**— IceCube [56] is a neutrino observatory located deep inside the Antarctic ice at the South Pole. The detector consists of 5,160 Digital Optical Modules (DOMs) deployed along 86 vertical strings below about 1.5 km of ice. The DOMs detect the Cherenkov photons emitted by the secondary charged particles that are produced during the interactions of neutrinos with ice. The  $\nu_\mu$  CC interactions produce muons which deposit energies in the form of long tracks, whereas  $\nu_e$  CC,  $\nu_\tau$  CC, and the NC interactions of neutrinos of all flavors deposit energies in the form of cascades. Some  $\nu_\tau$  CC events may also give rise to muons from the tau decay, resulting in tracks. Since the neutrino and antineutrino events have similar topologies, we perform our analysis without distinguishing them.

DeepCore is a densely instrumented central region of IceCube having DOMs with higher quantum efficiency. The reduced spacing between the neighboring DOMs in DeepCore, along with the enhanced DOM efficiency, helps DeepCore in detecting lower-energy neutrinos in the multi-GeV range. In the present analysis, we use the 8-year data sample of atmospheric neutrinos of high-

purity  $\nu_\mu$  CC events observed at DeepCore in the reconstructed energy range of 6.3 GeV to 158.5 GeV [55]. This dataset, consisting of 21914 events, corresponds to a “golden event sample”, where only those events are reconstructed that consist of direct photon hits without significant scattering in ice. Also, this sample is provided with the Monte Carlo (MC) events simulated using the full IceCube simulation chain [57]. Each event can be weighted to take into account the atmospheric neutrino flux [58], neutrino interaction cross section in the detector, three-flavor neutrino oscillations, and detector response such that the simulated sample accurately matches the experimentally observed data.

This golden event sample has been updated with the improved simulation, calibration, selection techniques, and reconstruction algorithms as described in detail in Ref. [59]. The selection criteria, filters, and reconstruction algorithms are developed using the simulated events, and the same are applied to the observed data to perform the analysis. Various kinds of filters have been applied to suppress the backgrounds like cosmic muons and detector noise, below 1% to obtain the neutrino-dominated sample.

Reconstruction algorithms based on the maximum likelihood technique have been employed to reconstruct observables like energy ( $E_{\text{reco}}$ ) and direction ( $\cos \theta_{\text{reco}}$ ) of a neutrino event. A particle identification (PID) score for each neutrino event is estimated using a Boosted Decision Tree (BDT). The PID score represents the probability of an event having the track-like topology. In this sample, the data is binned such that  $E_{\text{reco}}$  has 10 logarithmic bins in the range 6.3 GeV to 158.5 GeV and  $\cos \theta_{\text{reco}}$  has 10 linear bins in the range  $-1$  to  $0.1$ . To retain the sufficient statistics, the last energy bin is defined with twice the usual bin-width. According to the event topologies, the events are further categorized into two PID bins: mixed events ( $0.25 - 0.55$ ) and track-like events ( $0.55 - 1.0$ ). The cascade-like events with  $\text{PID} < 0.25$  have been removed by the collaboration to obtain the high-purity  $\nu_\mu$  CC sample; hence, those events are not present in the sample.

To study the effects of NSI on expected events at DeepCore, we show the distributions of event difference between SI + NSI and SI scenarios in Fig. 3. These distributions indicate the regions in reconstructed energy and cosine zenith that contribute most to the sensitivity. In the top panels, we take the NSI with a benchmark value of  $\varepsilon_{\mu\tau} = +0.05$ , considering other NSI parameters to be zero, where the event differences occur with alternating signs around the oscillation valley up to the high energy region. In the bottom panels, we take NSI with  $\varepsilon_{\tau\tau} - \varepsilon_{\mu\mu} = +0.1$ , considering other NSI parameters to be zero, where the event differences occur only in the positive direction. These features are consistent with those observed in the probability oscillograms on the left panels of Fig. 2, which demonstrate the fidelity of the detector in retaining the effects of NSI on the oscillation patterns even after considering all neutrino flavors,

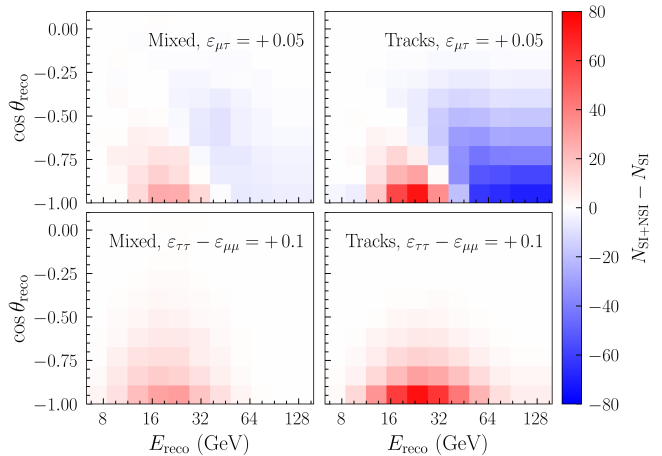


FIG. 3. Difference of the expected event distributions between SI + NSI and SI scenarios (*i.e.*,  $N_{\text{SI+NSI}} - N_{\text{SI}}$ ) in the plane of the reconstructed energy  $E_{\text{reco}}$  and the reconstructed cosine of zenith angle  $\cos \theta_{\text{reco}}$ , for two NSI parameter choices taken one at a time. The top and bottom panels correspond to  $\varepsilon_{\mu\tau} = +0.05$  and  $\varepsilon_{\tau\tau} - \varepsilon_{\mu\mu} = +0.1$ , respectively. The left and right panels show distributions for mixed and track-like samples, respectively. Here, we use the nominal values of the nuisance parameters as given in Table A1.

interaction kinematics, and the detector response. The distributions of event difference for the negative values of these NSI parameters are discussed in the Supplemental Material.

**Numerical analysis.**— This analysis constrains the NSI parameters  $\varepsilon_{\mu\tau}$  and  $\varepsilon_{\tau\tau} - \varepsilon_{\mu\mu}$  using a binned  $\chi^2$  approach, where each NSI parameter is constrained independently one at a time while keeping the other NSI parameters fixed to zero. The statistical analysis based on the Frequentist method is performed by calculating the binned  $\chi^2$  between the observed and expected event counts in bins of reconstructed energy, cosine zenith, and PID. For this analysis, the test statistic is adapted from Ref. [60]

$$\chi_{\text{mod}}^2 = \sum_{i \in \text{bins}} \frac{(N_i^{\text{exp}} - N_i^{\text{obs}})^2}{N_i^{\text{exp}} + (\sigma_i^{\text{sim}})^2} + \sum_{j \in \text{syst}} \frac{(s_j - \hat{s}_j)^2}{\sigma_{s_j}^2}, \quad (3)$$

where  $N_i^{\text{exp}}$  is the expected event count in the  $i^{\text{th}}$  bin, which is the sum of the MC event weights.  $N_i^{\text{obs}}$  is the observed event counts in the  $i^{\text{th}}$  bin. The term  $\sigma_i^{\text{sim}}$  accounts for the statistical uncertainty in the MC simulations that is used to calculate  $N_i^{\text{exp}}$ . The second term is the penalty term to account for the prior information about the systematic uncertainties, where  $s_j$  is the value of the  $j^{\text{th}}$  systematic parameter,  $\hat{s}_j$  is its nominal value, and  $\sigma_{s_j}$  is the associated uncertainty.

The systematic uncertainties are incorporated in the analysis in the form of nuisance parameters by reweighting the expected MC events. The reweighting and the

binned  $\chi^2_{\text{mod}}$  calculations are performed using the open-source analysis framework PISA [61] provided by the IceCube collaboration. This analysis includes a total of 20 nuisance parameters, which are allowed to vary freely during the minimization of the  $\chi^2_{\text{mod}}$  function given in Eqn. 3. These nuisance parameters account for uncertainties arising from detector response, atmospheric neutrino flux, neutrino interaction cross section, atmospheric muon background, and the oscillation parameters  $\theta_{23}$  and  $\Delta m_{31}^2$  following the systematic treatment described in detail in Ref. [59]. The remaining oscillation parameters are fixed to their best-fit values obtained from NuFit v5.2 [62], except for  $\delta_{\text{CP}}$ , which is fixed to zero since its impact is negligible. The details of the systematic uncertainty parameters and their best-fit values obtained from the present analysis are provided in the Supplemental Material (see Table A1).

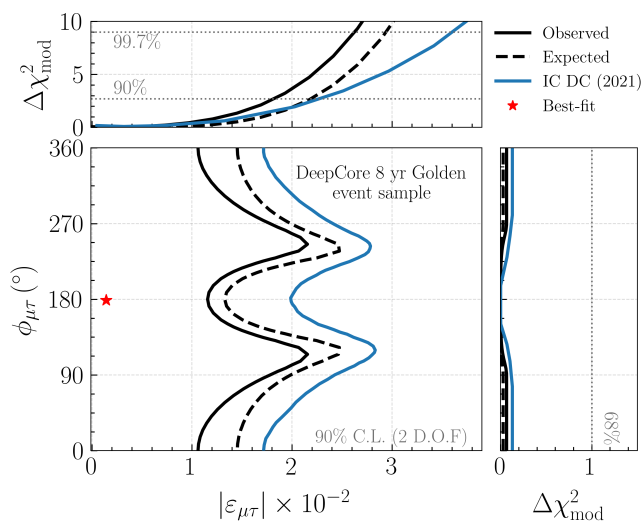


FIG. 4. The observed (black-solid curve) and the expected (black-dashed curve) constraints on the magnitude  $|\varepsilon_{\mu\tau}|$  and complex phase  $\phi_{\mu\tau}$  at the 90% C.L. (2 DOF) using the 8-year golden event sample of DeepCore. The red star marker represents the best-fit values for magnitude and phase. The top and the side sub-panels represent the 1D projections of the 2D contours for  $|\varepsilon_{\mu\tau}|$  and  $\phi_{\mu\tau}$ , respectively, while the  $\chi^2$  is minimized over the other parameter. The gray dotted lines in the sub-panels represent the 68.3%, 90%, and 99.7% confidence levels for 1 DOF. The solid blue curves represent the previous IceCube DeepCore result [44].

**Results.**— Figure 4 shows the 90% C.L. allowed regions considering 2 degrees of freedom (DOF) for the magnitude ( $|\varepsilon_{\mu\tau}|$ ) and phase ( $\phi_{\mu\tau}$ ) of the NSI parameter  $\varepsilon_{\mu\tau}$  using the 8-year golden event sample. The best-fit values of the magnitude and phase after fitting the data are 0.0014 and  $178.8^\circ$ , respectively, as shown by the red star. The  $\Delta\chi^2_{\text{mod}}$  for the best fit relative to the standard interaction is 0.06, indicating the data to be consistent with the standard interaction hypothesis with no NSI. The p-value of the NSI fit is 0.25, indicating good consistency of MC with the data (see Fig. C1 in the Supplemental

Material for comparison). The black-solid contour denotes the observed constraint at 90% C.L., while the black-dashed contour represents the expected sensitivity by taking the best-fit values as the truth. For comparison, the contour from the previous IceCube DeepCore (2021) result [44] is also included as the blue curve. The observed and expected 90% C.L. contours are in good agreement and are compatible with the previous IceCube DeepCore bounds [44]. The weak exclusion regions near  $90^\circ$  and  $270^\circ$  arise from the dependence of probability  $P(\nu_\mu \rightarrow \nu_\mu)$  on the term  $|\varepsilon_{\mu\tau}| \cos \phi_{\mu\tau}$  [18], which suppresses sensitivity in those regions. The top (side) sub-panel displays the one-dimensional projection of the magnitude (phase), which is obtained by minimizing  $\Delta\chi^2_{\text{mod}}$  over phase (magnitude). Using the 1D-projection, we obtain an upper bound of  $|\varepsilon_{\mu\tau}| \leq 0.018$  at 90% C.L., which is the most stringent among all existing constraints on this parameter. No constraint could be placed on the phase because the fitted magnitude goes to zero, resulting in no sensitivity to the phase.

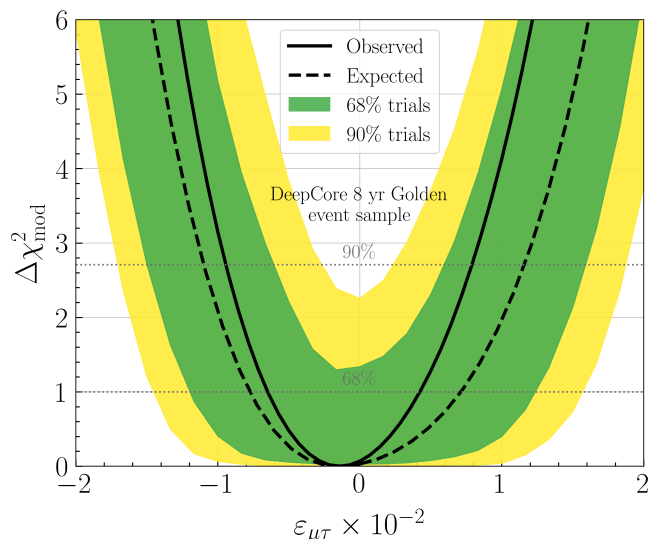


FIG. 5. The observed (black-solid curve) and the expected (black-dashed curve)  $\Delta\chi^2_{\text{mod}}$  as a function of the  $\varepsilon_{\mu\tau}$  parameter, assuming real values with the complex phase fixed to 0 and  $\pi$ . We use the 8-year golden event sample of DeepCore. Shaded bands show the 68% and 90% ranges for the expected  $\Delta\chi^2_{\text{mod}}$  calculated from 500 statistically fluctuated pseudo-experiments. The horizontal dotted lines represent the 68% and 90% confidence levels for 1 DOF.

To compare the constraints on the NSI parameter  $\varepsilon_{\mu\tau}$  obtained from this analysis with those from other experiments (shown in Fig. 1), the parameter has been scanned assuming real values by fixing the phase  $\phi_{\mu\tau}$  to 0 (*i.e.*, positive  $\varepsilon_{\mu\tau}$ ) and  $\pi$  (*i.e.*, negative  $\varepsilon_{\mu\tau}$ ). Figure 5 shows the observed (black-solid curve) and the expected (black-dashed curve)  $\Delta\chi^2_{\text{mod}}$  profiles for the real  $\varepsilon_{\mu\tau}$ . The 90% C.L. allowed range is found to be  $[-0.0094, 0.0079]$  which is the most stringent bound obtained from any neutrino oscillation experiment to date. The observed and

the expected curves are consistent with  $\Delta\chi^2$  distributions (bands) estimated from the statistically fluctuated pseudo-experiments within the  $1\sigma$  band.

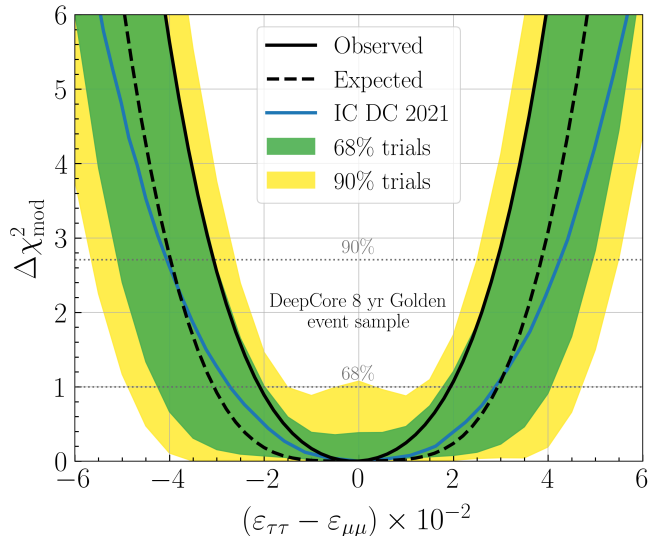


FIG. 6. The observed (black-solid curve) and the expected (black-dashed curve)  $\Delta\chi^2$  scan of NSI parameter  $\varepsilon_{\tau\tau} - \varepsilon_{\mu\mu}$  using the 8-year golden event sample of DeepCore. Shaded bands show the 68% and 90% ranges of the expected  $\Delta\chi^2$  calculated from 500 statistically fluctuated pseudo-experiments. The blue curve represents the  $\Delta\chi^2$  from the previous IceCube DeepCore result [44]. The horizontal dotted lines represent the 68% and 90% confidence levels for 1 DOF.

Figure 6 shows the observed (black-solid curve) and the expected (black-dashed curve)  $\Delta\chi^2_{\text{mod}}$  profiles for the non-universal NSI parameter  $\varepsilon_{\tau\tau} - \varepsilon_{\mu\mu}$ . The best-fit value of  $\varepsilon_{\tau\tau} - \varepsilon_{\mu\mu}$  is found to be  $-0.0009$ , with a  $\Delta\chi^2_{\text{mod}}$  of  $0.0017$  relative to the standard interaction scenario. This indicates that the observed data are fully compatible with the standard interaction hypothesis and show no evidence for NSI. The p-value of the NSI fit is  $0.25$ , indicating good consistency of MC with the data (see Fig. C1 in the Supplemental Material). The 90% C.L. allowed range from the observed  $\Delta\chi^2_{\text{mod}}$

profiles (black-solid curve) is  $[-0.030, 0.029]$ , which represents the strongest bound obtained from any neutrino oscillation experiment to date. The blue-solid curve represents the  $\Delta\chi^2_{\text{mod}}$  profile reported in the previous IceCube DeepCore analysis [44], demonstrating that the present result is consistent with the earlier measurement, while providing a stronger constraint. The observed  $\Delta\chi^2_{\text{mod}}$  profile is consistent with distributions of  $\Delta\chi^2_{\text{mod}}$  (bands) obtained from statistically fluctuated pseudo-experiments within the  $1\sigma$  band.

**Conclusion.**— In this work, we use the publicly available high-purity  $\nu_\mu$  CC golden event sample collected during 2011-2019 by IceCube DeepCore to probe the NC-NSI parameters  $\varepsilon_{\mu\tau}$  and  $\varepsilon_{\tau\tau} - \varepsilon_{\mu\mu}$ , which significantly affect the  $\nu_\mu$  disappearance channel. Our analysis shows that the dataset is consistent with the standard interaction hypothesis with no evidence for NSI. Exploiting the excellent sensitivity of this data sample to  $\nu_\mu$  disappearance channel, our analysis provides the most stringent bounds to date on  $\varepsilon_{\mu\tau}$  and  $\varepsilon_{\tau\tau} - \varepsilon_{\mu\mu}$ . Despite operating in the challenging conditions of the Antarctic ice, the IceCube DeepCore detector has maintained its stable performance and continues to provide high-quality data, which helps us to place competitive constraints on these NSI parameters. The IceCube Upgrade [63, 64] currently being deployed is expected to further constrain these NSI parameters using its improved systematics, better reconstruction, and high statistics with lower energy threshold.

**Acknowledgment.**— S.K.A., J.K., and A.K. acknowledge support from the Department of Atomic Energy (DAE), Govt. of India, and the Swarnajayanti Fellowship (Sanction Order No. DST/SJF/PSA-05/2019-20) provided by the Department of Science and Technology (DST), Govt. of India, and the Research Grant (Sanction Order No. SB/SJF/2020-21/21) provided by the Anusandhan National Research Foundation (ANRF), Govt. of India, under the Swarnajayanti Fellowship. The numerical simulations are performed using the Dell PowerEdge R660 Server and the “SAMKHYA: High-Performance Computing Facility” at the Institute of Physics, Bhubaneswar, India.

- 
- [1] Y. Fukuda *et al.* (Super-Kamiokande), Evidence for oscillation of atmospheric neutrinos, *Phys. Rev. Lett.* **81**, 1562 (1998), arXiv:hep-ex/9807003.
  - [2] Q. R. Ahmad *et al.* (SNO), Measurement of the rate of  $\nu_e + d \rightarrow p + p + e^-$  interactions produced by  $^8\text{B}$  solar neutrinos at the Sudbury Neutrino Observatory, *Phys. Rev. Lett.* **87**, 071301 (2001), arXiv:nucl-ex/0106015.
  - [3] Q. R. Ahmad *et al.* (SNO), Direct evidence for neutrino flavor transformation from neutral current interactions in the Sudbury Neutrino Observatory, *Phys. Rev. Lett.* **89**, 011301 (2002), arXiv:nucl-ex/0204008.
  - [4] S. Navas *et al.* (Particle Data Group), Review of particle physics, *Phys. Rev. D* **110**, 030001 (2024).
  - [5] I. Esteban, M. C. Gonzalez-Garcia, M. Maltoni, I. Martinez-Soler, J. P. Pinheiro, and T. Schwetz, NuFit-6.0: updated global analysis of three-flavor neutrino oscillations, *JHEP* **12**, 216, arXiv:2410.05380 [hep-ph].
  - [6] F. Capozzi, E. Lisi, F. Marcone, A. Marrone, and A. Palazzo, Updated bounds on the (1,2) neutrino oscillation parameters after first JUNO results, (2025), arXiv:2511.21650 [hep-ph].
  - [7] R. Abbasi *et al.* (IceCube), The Design and Performance

- of IceCube DeepCore, *Astropart. Phys.* **35**, 615 (2012), [arXiv:1109.6096 \[astro-ph.IM\]](#).
- [8] Y. Fukuda *et al.* (Super-Kamiokande), The Super-Kamiokande detector, *Nucl. Instrum. Meth. A* **501**, 418 (2003).
- [9] S. Weinberg, A Model of Leptons, *Phys. Rev. Lett.* **19**, 1264 (1967).
- [10] M. B. Gavela, D. Hernandez, T. Ota, and W. Winter, Large gauge invariant non-standard neutrino interactions, *Phys. Rev. D* **79**, 013007 (2009), [arXiv:0809.3451 \[hep-ph\]](#).
- [11] I. Bischer and W. Rodejohann, General neutrino interactions from an effective field theory perspective, *Nucl. Phys. B* **947**, 114746 (2019), [arXiv:1905.08699 \[hep-ph\]](#).
- [12] L. Wolfenstein, Neutrino Oscillations in Matter, *Phys. Rev. D* **17**, 2369 (1978).
- [13] J. Valle, Resonant Oscillations of Massless Neutrinos in Matter, *Phys. Lett. B* **199**, 432 (1987).
- [14] M. M. Guzzo, A. Masiero, and S. T. Petcov, On the MSW effect with massless neutrinos and no mixing in the vacuum, *Phys. Lett. B* **260**, 154 (1991).
- [15] M. M. Guzzo, H. Nunokawa, P. C. de Holanda, and O. L. G. Peres, On the massless 'just-so' solution to the solar neutrino problem, *Phys. Rev. D* **64**, 097301 (2001), [arXiv:hep-ph/0012089](#).
- [16] P. Huber and J. W. F. Valle, Nonstandard interactions: Atmospheric versus neutrino factory experiments, *Phys. Lett. B* **523**, 151 (2001), [arXiv:hep-ph/0108193 \[hep-ph\]](#).
- [17] M. C. Gonzalez-Garcia and M. Maltoni, Atmospheric neutrino oscillations and new physics, *Phys. Rev. D* **70**, 033010 (2004), [arXiv:hep-ph/0404085](#).
- [18] J. Kopp, M. Lindner, T. Ota, and J. Sato, Non-standard neutrino interactions in reactor and superbeam experiments, *Phys. Rev. D* **77**, 013007 (2008), [arXiv:0708.0152 \[hep-ph\]](#).
- [19] C. Biggio, M. Blennow, and E. Fernandez-Martinez, General bounds on non-standard neutrino interactions, *JHEP* **08**, 090, [arXiv:0907.0097 \[hep-ph\]](#).
- [20] F. J. Escrihuela, M. Tortola, J. W. F. Valle, and O. G. Miranda, Global constraints on muon-neutrino non-standard interactions, *Phys. Rev. D* **83**, 093002 (2011), [arXiv:1103.1366 \[hep-ph\]](#).
- [21] M. C. Gonzalez-Garcia, M. Maltoni, and J. Salvado, Testing matter effects in propagation of atmospheric and long-baseline neutrinos, *JHEP* **05**, 075, [arXiv:1103.4365 \[hep-ph\]](#).
- [22] S. K. Agarwalla, F. Lombardi, and T. Takeuchi, Constraining Non-Standard Interactions of the Neutrino with Borexino, *JHEP* **12**, 079, [arXiv:1207.3492 \[hep-ph\]](#).
- [23] T. Ohlsson, Status of non-standard neutrino interactions, *Rept. Prog. Phys.* **76**, 044201 (2013), [arXiv:1209.2710 \[hep-ph\]](#).
- [24] A. Esmaili and A. Y. Smirnov, Probing Non-Standard Interaction of Neutrinos with IceCube and DeepCore, *JHEP* **06**, 026, [arXiv:1304.1042 \[hep-ph\]](#).
- [25] M. C. Gonzalez-Garcia and M. Maltoni, Determination of matter potential from global analysis of neutrino oscillation data, *JHEP* **09**, 152, [arXiv:1307.3092 \[hep-ph\]](#).
- [26] P. Adamson *et al.* (MINOS), Search for Flavor-Changing Non-Standard Neutrino Interactions by MINOS, *Phys. Rev. D* **88**, 072011 (2013), [arXiv:1303.5314 \[hep-ex\]](#).
- [27] A. Chatterjee, P. Mehta, D. Choudhury, and R. Gandhi, Testing nonstandard neutrino matter interactions in atmospheric neutrino propagation, *Phys. Rev. D* **93**, 093017 (2016), [arXiv:1409.8472 \[hep-ph\]](#).
- [28] S. K. Agarwalla, P. Bagchi, D. V. Forero, and M. Tórtola, Probing Non-Standard Interactions at Daya Bay, *JHEP* **07**, 060, [arXiv:1412.1064 \[hep-ph\]](#).
- [29] I. Mocioiu and W. Wright, Non-standard neutrino interactions in the mu-tau sector, *Nucl. Phys. B* **893**, 376 (2015), [arXiv:1410.6193 \[hep-ph\]](#).
- [30] O. G. Miranda and H. Nunokawa, Non standard neutrino interactions: current status and future prospects, *New J. Phys.* **17**, 095002 (2015), [arXiv:1505.06254 \[hep-ph\]](#).
- [31] S. K. Agarwalla, Y. Kao, D. Saha, and T. Takeuchi, Running of Oscillation Parameters in Matter with Flavor-Diagonal Non-Standard Interactions of the Neutrino, *JHEP* **11**, 035, [arXiv:1506.08464 \[hep-ph\]](#).
- [32] S. Choubey, A. Ghosh, T. Ohlsson, and D. Tiwari, Neutrino Physics with Non-Standard Interactions at INO, *JHEP* **12**, 126, [arXiv:1507.02211 \[hep-ph\]](#).
- [33] S. K. Agarwalla, S. S. Chatterjee, and A. Palazzo, Degeneracy between  $\theta_{23}$  octant and neutrino non-standard interactions at DUNE, *Phys. Lett. B* **762**, 64 (2016), [arXiv:1607.01745 \[hep-ph\]](#).
- [34] J. Salvado, O. Mena, S. Palomares-Ruiz, and N. Rius, Non-standard interactions with high-energy atmospheric neutrinos at IceCube, *JHEP* **01**, 141, [arXiv:1609.03450 \[hep-ph\]](#).
- [35] Y. Farzan and M. Tortola, Neutrino oscillations and Non-Standard Interactions, *Front.in Phys.* **6**, 10 (2018), [arXiv:1710.09360 \[hep-ph\]](#).
- [36] P. Coloma, P. B. Denton, M. C. Gonzalez-Garcia, M. Maltoni, and T. Schwetz, Curtailing the Dark Side in Non-Standard Neutrino Interactions, *JHEP* **04**, 116, [arXiv:1701.04828 \[hep-ph\]](#).
- [37] M. G. Aartsen *et al.* (IceCube), Search for Nonstandard Neutrino Interactions with IceCube DeepCore, *Phys. Rev. D* **97**, 072009 (2018), [arXiv:1709.07079 \[hep-ex\]](#).
- [38] I. Esteban, M. C. Gonzalez-Garcia, M. Maltoni, I. Martinez-Soler, and J. Salvado, Updated constraints on non-standard interactions from global analysis of oscillation data, *JHEP* **08**, 180, [Addendum: *JHEP* **12**, 152 (2020)], [arXiv:1805.04530 \[hep-ph\]](#).
- [39] S. K. Agarwalla *et al.* (Borexino), Constraints on flavor-diagonal non-standard neutrino interactions from Borexino Phase-II, *JHEP* **02**, 038, [arXiv:1905.03512 \[hep-ph\]](#).
- [40] P. S. Bhupal Dev *et al.*, Neutrino Non-Standard Interactions: A Status Report, *SciPost Phys. Proc.* **2**, 001 (2019), [arXiv:1907.00991 \[hep-ph\]](#).
- [41] A. Khatun, S. S. Chatterjee, T. Thakore, and S. Kumar Agarwalla, Enhancing sensitivity to non-standard neutrino interactions at INO combining muon and hadron information, *Eur. Phys. J. C* **80**, 533 (2020), [arXiv:1907.02027 \[hep-ph\]](#).
- [42] A. Kumar, A. Khatun, S. K. Agarwalla, and A. Dighe, A New Approach to Probe Non-Standard Interactions in Atmospheric Neutrino Experiments, *JHEP* **04**, 159, [arXiv:2101.02607 \[hep-ph\]](#).
- [43] S. K. Agarwalla, S. Das, M. Masud, and P. Swain, Evolution of neutrino mass-mixing parameters in matter with non-standard interactions, *JHEP* **11**, 094, [arXiv:2103.13431 \[hep-ph\]](#).
- [44] R. Abbasi *et al.* (IceCube), All-flavor constraints on non-standard neutrino interactions and generalized matter potential with three years of IceCube DeepCore data, *Phys. Rev. D* **104**, 072006 (2021), [arXiv:2106.07755 \[hep-ex\]](#).

- [45] J. Krishnamoorthi, A. K. Upadhyay, A. Kumar, and S. K. Agarwalla, Probing earth's core using atmospheric neutrino oscillations in the presence of  $\nu_s$  at ino-ical, *JHEP* **2025** (10), [arXiv:2507.02167 \[hep-ph\]](#).
- [46] P. Coloma, M. C. Gonzalez-Garcia, M. Maltoni, J. P. Pinheiro, and S. Urrea, Global constraints on non-standard neutrino interactions with quarks and electrons, *JHEP* **08**, 032, [arXiv:2305.07698 \[hep-ph\]](#).
- [47] M. A. Acero *et al.* (NOvA), Search for CP-Violating Neutrino Nonstandard Interactions with the NOvA Experiment, *Phys. Rev. Lett.* **133**, 201802 (2024), [arXiv:2403.07266 \[hep-ex\]](#).
- [48] S. Aiello *et al.* (KM3NeT), Search for non-standard neutrino interactions with the first six detection units of KM3NeT/ORCA, *JCAP* **02**, 073, [arXiv:2411.19078 \[hep-ex\]](#).
- [49] A. Albert *et al.* (ANTARES), Search for non-standard neutrino interactions with 10 years of ANTARES data, *JHEP* **07**, 048, [arXiv:2112.14517 \[hep-ex\]](#).
- [50] R. Abbasi *et al.* (IceCube), Strong Constraints on Neutrino Nonstandard Interactions from TeV-Scale  $\nu_u$  Disappearance at IceCube, *Phys. Rev. Lett.* **129**, 011804 (2022), [arXiv:2201.03566 \[hep-ex\]](#).
- [51] G. Mitsuka *et al.* (Super-Kamiokande), Study of Non-Standard Neutrino Interactions with Atmospheric Neutrino Data in Super-Kamiokande I and II, *Phys. Rev. D* **84**, 113008 (2011), [arXiv:1109.1889 \[hep-ex\]](#).
- [52] Z. Maki, M. Nakagawa, and S. Sakata, Remarks on the unified model of elementary particles, *Prog. Theor. Phys.* **28**, 870 (1962).
- [53] R. Opher, Coherent scattering of cosmic neutrinos, *Astron. Astrophys.* **37**, 135 (1974).
- [54] P. Langacker, J. P. Leveille, and J. Sheiman, On the Detection of Cosmological Neutrinos by Coherent Scattering, *Phys. Rev. D* **27**, 1228 (1983).
- [55] R. Abbasi *et al.* (IceCube), [Replication Data for: Measurement of atmospheric neutrino mixing with improved IceCube DeepCore calibration and data processing](#) (2025).
- [56] M. G. Aartsen *et al.* (IceCube), The IceCube Neutrino Observatory: Instrumentation and Online Systems, *JINST* **12** (03), P03012, [Erratum: *JINST* 19, E05001 (2024)], [arXiv:1612.05093 \[astro-ph.IM\]](#).
- [57] M. G. Aartsen *et al.* (IceCube), Measurement of Atmospheric Tau Neutrino Appearance with IceCube DeepCore, *Phys. Rev. D* **99**, 032007 (2019), [arXiv:1901.05366 \[hep-ex\]](#).
- [58] M. Honda, M. Sajjad Athar, T. Kajita, K. Kasahara, and S. Midorikawa, Atmospheric neutrino flux calculation using the NRLMSISE-00 atmospheric model, *Phys. Rev. D* **92**, 023004 (2015), [arXiv:1502.03916 \[astro-ph.HE\]](#).
- [59] R. Abbasi *et al.* (IceCube), Measurement of atmospheric neutrino mixing with improved IceCube DeepCore calibration and data processing, *Phys. Rev. D* **108**, 012014 (2023), [arXiv:2304.12236 \[hep-ex\]](#).
- [60] M. G. Aartsen *et al.* (IceCube), Measurement of Atmospheric Neutrino Oscillations at 6–56 GeV with IceCube DeepCore, *Phys. Rev. Lett.* **120**, 071801 (2018), [arXiv:1707.07081 \[hep-ex\]](#).
- [61] M. G. Aartsen *et al.* (IceCube), Computational techniques for the analysis of small signals in high-statistics neutrino oscillation experiments, *Nucl. Instrum. Meth. A* **977**, 164332 (2020), [arXiv:1803.05390 \[physics.data-an\]](#).
- [62] I. Esteban, M. C. Gonzalez-Garcia, M. Maltoni, T. Schwetz, and A. Zhou, The fate of hints: updated global analysis of three-flavor neutrino oscillations, *JHEP* **09**, 178, [arXiv:2007.14792 \[hep-ph\]](#).
- [63] A. Ishihara (IceCube), The IceCube Upgrade - Design and Science Goals, *PoS ICRC2019*, 1031 (2021), [arXiv:1908.09441 \[astro-ph.HE\]](#).
- [64] R. Abbasi *et al.* (IceCube), Physics potential of the IceCube Upgrade for atmospheric neutrino oscillations, (2025), [arXiv:2509.13066 \[hep-ex\]](#).
- [65] G. D. Barr, T. K. Gaisser, S. Robbins, and T. Stanev, Uncertainties in Atmospheric Neutrino Fluxes, *Phys. Rev. D* **74**, 094009 (2006), [arXiv:astro-ph/0611266](#).

## Supplemental Material for

### *Stringent constraints on non-standard neutrino interactions using high-purity $\nu_\mu$ CC events in IceCube DeepCore*

#### Appendix A: Systematic uncertainties

This analysis follows the systematic uncertainty treatment described in Ref. [59], where we incorporate uncertainties related to the detector response, atmospheric neutrino flux, neutrino interaction cross section, normalization, and neutrino oscillations. Among the detector-related parameters, the uncertainty in the overall optical efficiency of the DOMs is represented by a single scaling parameter. The ice absorption and ice scattering parameters account for variations in the absorption and scattering lengths of the bulk ice. Two additional parameters,  $p_0$  and  $p_1$ , describe the relative angular acceptance of the optical modules, accounting for changes in the optical properties of refrozen ice along each string column.

Atmospheric neutrino flux predictions are based on the model from Ref. [58]. The associated uncertainties include the spectral index parameter ( $\Delta\gamma_\nu$ ) and uncertainties related to the production of pions and kaons, following the method provided in Ref. [65]. Uncertainties in the neutrino-nucleon interaction cross sections are parameterized through the axial mass parameters corresponding to the quasi-elastic (QE) and the resonant (RES) interactions. For Deep Inelastic Scattering (DIS) interactions, an interpolated model between GENIE and CSMS predictions is used. An additional normalization parameter is included to account for uncertainties in the NC-type event rate. Apart from these parameters, overall normalization parameters for the neutrinos and the atmospheric muon background are also included. In the set of neutrino oscillation parameters, the uncertainties from  $\theta_{23}$  and  $\Delta m_{31}^2$  are also considered in this work.

The list of systematic uncertainty parameters, along with their corresponding nominal values,  $1\sigma$  priors and ranges, is summarized in Table A1. A pull penalty term is added to  $\chi^2_{\text{mod}}$  for the parameters where priors are available. Parameters without priors are assumed to follow uniform distributions with no pull penalty. The table also reports the best-fit values of the systematic parameters obtained from the two independent fits for SI + NSI scenarios - one for  $\varepsilon_{\mu\tau}$  and another for  $\varepsilon_{\tau\tau} - \varepsilon_{\mu\mu}$ , taken one at a time with the other NSI parameters considered to be zero. The best-fit values of these nuisance parameters are found to be consistent between the two fits.

#### Appendix B: Effects of the NSI on DeepCore events

Figure B1 shows the distributions for event differences between the SI + NSI and the SI scenarios with the benchmark values of  $\varepsilon_{\mu\tau} = -0.05$  and  $\varepsilon_{\tau\tau} - \varepsilon_{\mu\mu} = -0.1$ .

The distributions of event differences highlight the re-

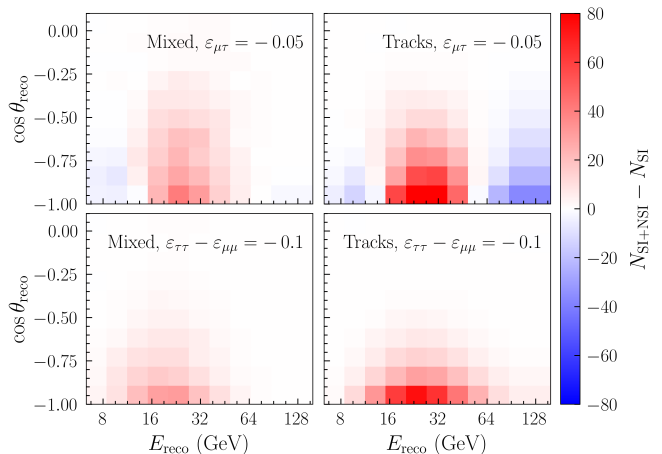


FIG. B1. Difference of the expected event distributions between SI + NSI and SI scenarios (*i.e.*,  $N_{\text{SI+NSI}} - N_{\text{SI}}$ ) in the plane of the reconstructed energy  $E_{\text{reco}}$  and the reconstructed cosine of zenith angle  $\cos \theta_{\text{reco}}$ , for two NSI parameter choices taken one at a time. The top and bottom panels correspond to  $\varepsilon_{\mu\tau} = -0.05$  and  $\varepsilon_{\tau\tau} - \varepsilon_{\mu\mu} = -0.1$ , respectively. The left and right panels show distributions for mixed and track-like samples, respectively. Here, we use the nominal values of the nuisance parameters as given in Table A1.

gions in reconstructed energy and cosine zenith that contribute significantly to the sensitivity for NSI. The top panels corresponding to  $\varepsilon_{\mu\tau} = -0.05$  show the event differences with alternating signs in the region of the oscillation valley up to the high-energy region, while the bottom panels corresponding to  $\varepsilon_{\tau\tau} - \varepsilon_{\mu\mu} = -0.1$  show event differences only in the positive direction below 100 GeV. From the comparison between Fig. 3 and Fig. B1, it can be observed that the shape of the signal region in the distribution of event difference changes with the sign of  $\varepsilon_{\mu\tau}$ . In contrast, for  $\varepsilon_{\tau\tau} - \varepsilon_{\mu\mu}$ , the signal region remains nearly identical irrespective of the sign of the parameter.

#### Appendix C: Data-MC Comparison

Figure C1 shows the comparison of the 1D projections of the observed data and the best-fit MC predictions for the NSI parameters  $\varepsilon_{\mu\tau}$  and  $\varepsilon_{\tau\tau} - \varepsilon_{\mu\mu}$  taken one at a time. The event distributions are shown as functions of the reconstructed energy (top panels) and the cosine zenith (bottom panels), separately for each PID. The best-fit MC predictions obtained from the independent fits for SI + NSI scenarios with  $\varepsilon_{\mu\tau}$  and  $\varepsilon_{\tau\tau} - \varepsilon_{\mu\mu}$  taken one at a time show good agreement with the observed data.

Parameter	Best-fit ( $\varepsilon_{\mu\tau}$ )	Best-fit ( $\varepsilon_{\tau\tau} - \varepsilon_{\mu\mu}$ )	Nominal value	Prior ( $1\sigma$ )	Range
<b>Detector:</b>					
DOM efficiency	1.064	1.064	1.0	$\pm 0.1$	[0.8, 1.2]
Ice absorption	0.973	0.973	1.0	-	[0.9, 1.1]
Ice scattering	0.987	0.987	1.05	-	[0.95, 1.15]
Relative eff. $p_0$	-0.271	-0.269	0.10	-	[-0.2, 0.6]
Relative eff. $p_1$	-0.043	-0.042	-0.05	-	[-0.2, 0.2]
<b>Atmospheric neutrino flux:</b>					
$\Delta\gamma_\nu$	0.063	0.063	0.0	$\pm 0.1$	[-0.5, 0.5]
$\Delta\pi^+$ yields [A-F]	0.06	0.06	0.0	$\pm 0.3$	[-1.5, 1.5]
$\Delta\pi^+$ yields G	-0.048	-0.05	0.0	$\pm 0.15$	[-1.5, 1.5]
$\Delta\pi^+$ yields H	-0.013	-0.017	0.0	$\pm 0.15$	[-0.75, 0.75]
$\Delta K^+$ yields W	0.078	0.084	0.0	$\pm 0.4$	[-0.20, 2.0]
$\Delta K^+$ yields Y	0.095	0.107	0.0	$\pm 0.3$	[-1.5, 1.5]
$\Delta K^-$ yields K	-0.012	-0.009	0.0	$\pm 0.4$	[-2.0, 2.0]
<b>Neutrino interaction cross section:</b>					
$M_A^{\text{CCQE}}$ (in $\sigma$ )	0.058	0.061	0.0	$\pm 1.0$	[-2.0, 2.0]
$M_A^{\text{CCRES}}$ (in $\sigma$ )	0.60	0.606	0.0	$\pm 1.0$	[-2.0, 2.0]
DIS CSMS	0.044	0.033	0.0	$\pm 1.0$	[-3.0, 3.0]
$\sigma_{\text{NC}}/\sigma_{\text{CC}}$	1.129	1.127	1.0	$\pm 0.2$	[0.5, 1.5]
<b>Normalization:</b>					
$A_{\text{eff}}$ scale	0.823	0.824	1.0	-	[0.6, 1.4]
<b>Atmospheric muons:</b>					
Atm. $\mu$ scale	1.349	1.364	1.0	-	[0.7, 1.5]
<b>Oscillations:</b>					
$\theta_{23}$	45.343 $^\circ$	45.326 $^\circ$	45.573 $^\circ$	-	[38 $^\circ$ , 52 $^\circ$ ]
$\Delta m_{31}^2$	0.002498 eV $^2$	0.002488 eV $^2$	0.002484 eV $^2$	-	[0.002, 0.003] eV $^2$

TABLE A1. The table shows the systematic uncertainty parameters considered as nuisance parameters in this analysis. The nominal value, associated  $1\sigma$  prior (if available), and the allowed range during minimization are mentioned for each parameter. The table also includes the best-fit values for these parameters obtained from the data fitting with the SI + NSI hypothesis having parameters  $\varepsilon_{\mu\tau}$  (second column) and  $\varepsilon_{\tau\tau} - \varepsilon_{\mu\mu}$  (third column) considered one at a time.

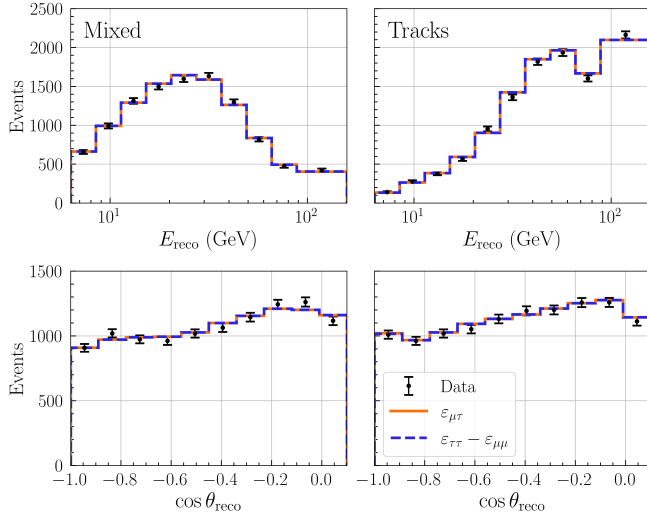


FIG. C1. Comparison of reconstructed event distributions between the observed data in the 8-year golden event sample of DeepCore and the best-fit MC predictions for different NSI scenarios as a function of energy  $E_{\text{reco}}$  (top panels) and the cosine of zenith angle  $\cos\theta_{\text{reco}}$  (bottom panels). The left and right panels correspond to the mixed and track-like event samples, respectively. The black dots denote the data with statistical uncertainties. The orange-solid and blue-dashed lines represent the best-fit MC predictions for the NSI scenarios with  $\varepsilon_{\mu\tau}$  and  $\varepsilon_{\tau\tau} - \varepsilon_{\mu\mu}$ , respectively, taken one at a time.